Supplement of Atmos. Chem. Phys., 18, 2199–2224, 2018
https://doi.org/10.5194/acp-18-2199-2018-supplement

Atmospheric Chemistry and Physics
Open Access
EGU

Supplement of

Bulk and molecular-level characterization of laboratory-aged biomass burning organic aerosol from oak leaf and heartwood fuels

Claire F. Fortenberry et al.

Correspondence to: Brent J. Williams (brentw@wustl.edu)

Section S1: Experimental Setup

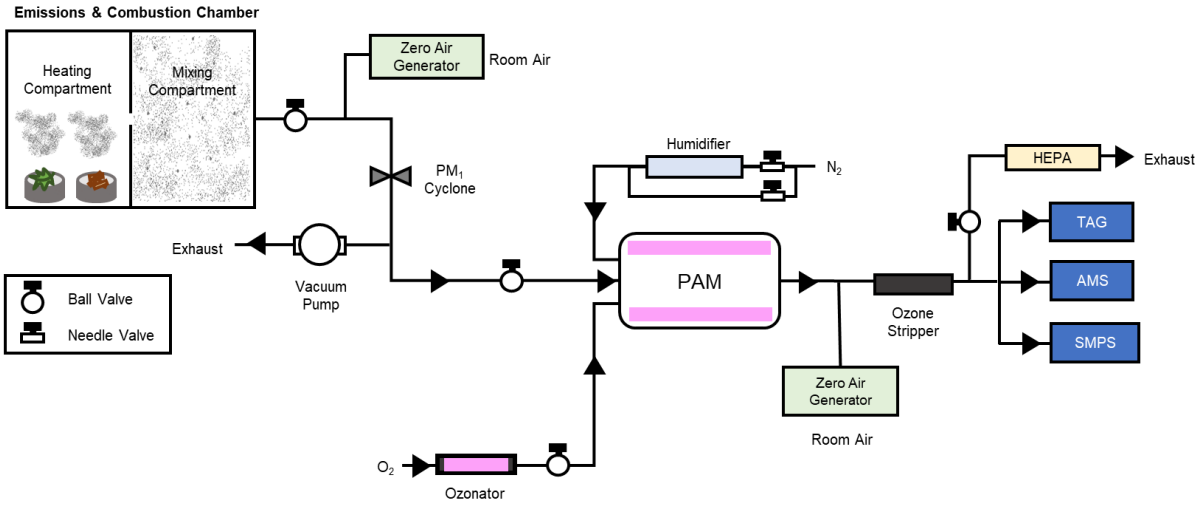

Figure S1: Flow diagram of experimental setup

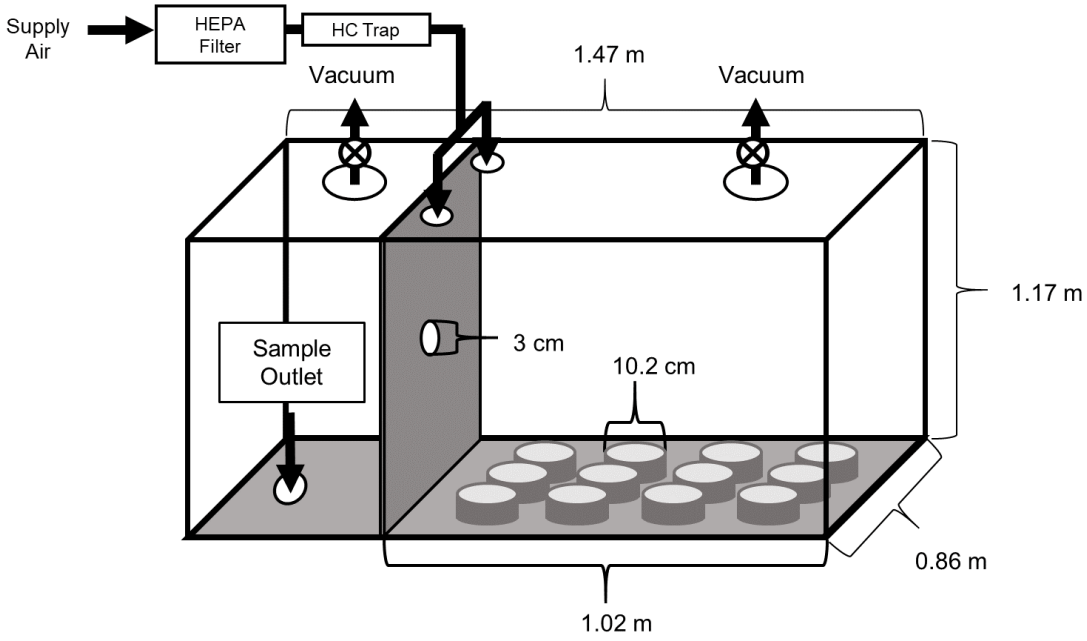

Figure S2: Diagram of emissions and combustion chamber. Further details are provided elsewhere (Mellott, 2012).

Section S2: PAM Calibrations, Equivalent Aging Estimations, and Gas Measurements

S2.1 SO_2 Calibrations

The PAM was calibrated a week prior to the first experimentation period. Equivalent atmospheric aging times were determined by calibrating the PAM reactor with sulfur dioxide (SO_2) gas, as described by Kang, et al (Kang et al., 2007). A constant stream of SO_2 (Airgas, Inc., Radnor, PA) was introduced into the PAM chamber at a steady flow rate of 0.02 L min^{-1}. Humidified N_2 (RH = 30%) and O_2 flow rates were maintained at 4.6 L min^{-1} and 0.4 L min^{-1}, respectively. The total flow rate through the PAM chamber was maintained at 10 L min^{-1} throughout the calibration. The PAM ultraviolet (UV) lamp voltage was systematically varied from 30 to 100V, and the SO_2 concentration was measured for 25 minutes at each setting using an SO_2 analyzer (Model 43i-TLE, Thermo Fisher Scientific, Waltham, MA). OH exposure (OH_{exp}), defined as the OH concentration multiplied by the reactor residence time, was calculated based on a pseudo-first order rate expression for the reaction of SO_2 with OH:

$$\frac{d[\mathrm{SO_2}]}{dt} = -k_{OH}[\mathrm{OH}][\mathrm{SO_2}]$$

$$\mathrm{OH_{exp}} = [\mathrm{OH}]t = \frac{1}{k_{OH}} ln\left(\frac{[\mathrm{SO_2}]_0}{[\mathrm{SO_2}]}\right)$$

where k_{OH} is the rate constant for the reaction of SO_2 with OH· (9×10^{-13} cm^3 $molec^{-1}$ s^{-1} ; Davis et al., 1979; Lambe et al., 2011) and $[SO_2]_0$ is the initial SO_2 concentration.

Equivalent aging times (t_{equiv}) were determined for each voltage setting assuming an average atmospheric OH· concentration ($[OH]_{atm}$) of 1.5×10^6 molec cm^{-3} (Mao et al., 2009) and a reactor residence time of 78 seconds:

$$t_{equiv} = \frac{[\mathrm{OH}]_{\mathrm{atm}}}{\mathrm{OH_{exp}}}$$

To obtain OH_{exp} and equivalent aging times for each PAM UV lamp setting, the results of the calibration were fit with a linear regression ($r^2 = 0.957$). OH_{exp} and equivalent aging time values are given as functions of the PAM light voltage in Figure S3a.

OH forms in the PAM reactor when monatomic oxygen radicals, produced as a result of O_3 UV (254 nm) photolysis, react with water molecules (Ehhalt et al., 1990; Lambe et al., 2011; Levy, 1971; Palm et al., 2016; Shetter et al., 1996). Previous PAM studies have demonstrated that OH· production increases with increasing relative humidity (RH) (Kang et al., 2007; Li et al., 2015; Peng et al., 2015, 2016). The sensitivity of OH_{exp} to RH in our PAM reactor was investigated by performing SO_2 calibrations at 10%, 20%, and 30% RH (Figure S3b).

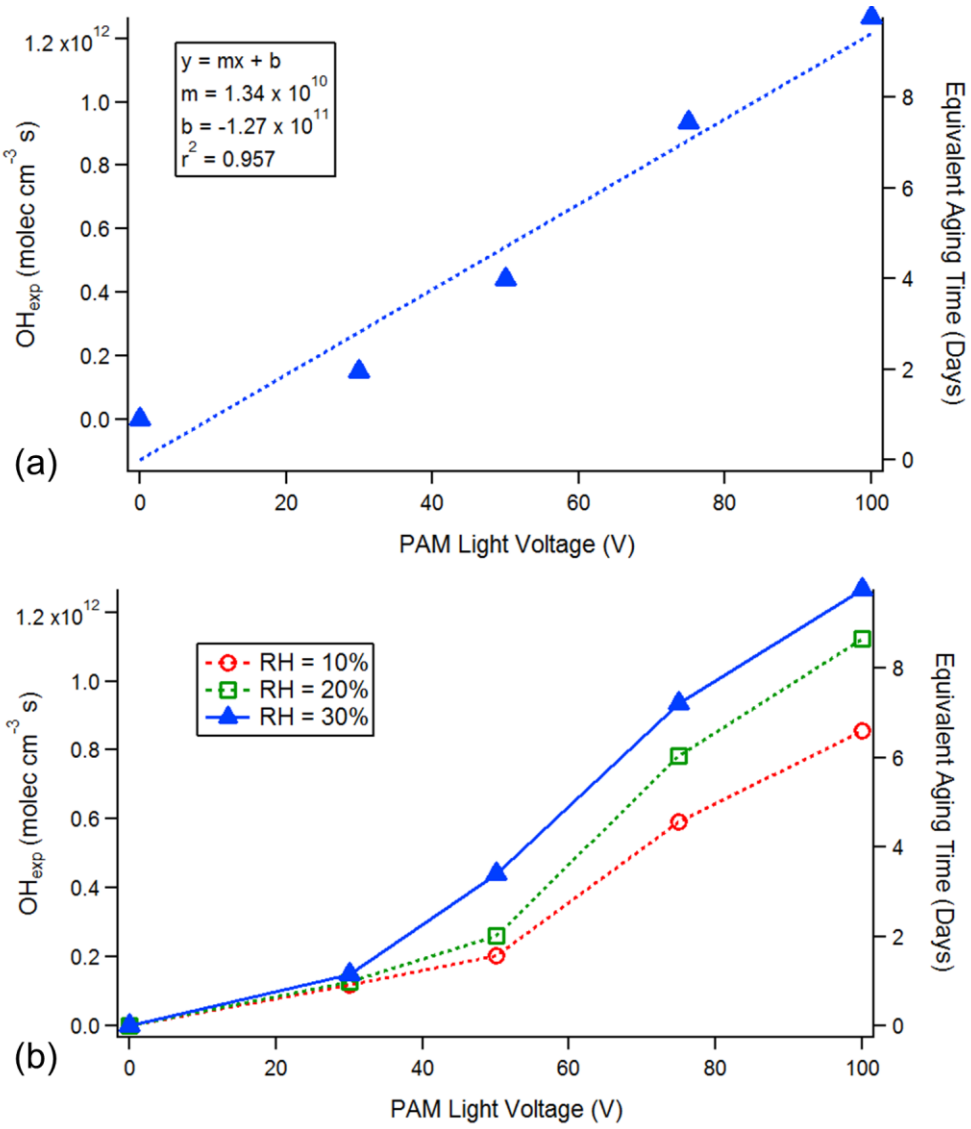

Figure S3. Results from PAM reactor SO_2 calibrations, displayed as OH_{exp} and equivalent aging times as functions of PAM reactor light voltage. **(a)** results from the calibration at RH = 30%, with linear regression parameters provided; **(b)** results from calibrations at 10% (red circles), 20% (green squares), and 30% (blue triangles) RH.

S2.2 Estimation of External OH Reactivity (OHR_{ext})

To better constrain the equivalent aging times characteristic of our system, additional emissions experiments were conducted to estimate OHR_{ext} (Peng et al., 2016). CO, which is recommended as a tracer for offline calibrations when high VOC concentrations are observed (Li et al., 2015), was used as a surrogate species to observe gas-phase oxidation in the PAM reactor. The emissions and combustion procedure was repeated for both leaf and heartwood fuels, and CO was measured using a trace-level CO monitor (Peak Laboratories, Mountain View, CA) that operated at 3-minute time resolution. Trace-level gas monitors were also used to monitor NO_x (Model 42i analyzer, Thermo Fisher Scientific, Waltham, MA) and O_3 (Model 43i TLE analyzer, Thermo Fisher Scientific, Waltham, MA) concentrations. Aerosol was sampled alternately every 12 minutes through the PAM reactor and through a bypass line to obtain CO measurements for aged and unaged emissions. During these experiments, the PAM lamp settings corresponded to approximately 3 equivalent days of aging according to the most recent offline calibration.

CO measurements are provided in figure S4. In the leaf BBOA, aged and unaged CO concentrations exhibited little variation, and calculated OHR_{ext} values for baseline-subtracted CO concentrations were similar between aging conditions (0.56 s^{-1} for PAM-aged emissions and 0.51 s^{-1} for unaged emissions). In the heartwood BBOA, CO concentrations did not exceed ambient chamber concentrations (≤130 ppb) and are therefore not presented here. Additionally, NO_x concentrations were low (<1 ppb) across all conditions for both fuel types and are therefore not considered significant.

To estimate total OHR_{ext}, we obtained emission factors (EFs) for relevant trace gas species from laboratory-generated "oak woodland" emissions (*Quercus emoryi* and *Arctostaphylos pungens*; Burling et al., 2010) and calculated ratios between gas EFs and the corresponding CO EF. Expected gas-phase concentrations were estimated by multiplying these ratios by CO concentrations measured in our experiments. Second-order OH rate constants were obtained using the NIST Chemical Kinetics Database (Manion et al., 2015; other references cited therein) and were used to calculate total OHR_{ext} using equation 1. From these calculations, we estimate a total OHR_{ext} of approximately 2.2 s^{-1} for both aged and unaged emissions. This value is used in subsequent OH_{exp} and equivalent aging time approximations.

This OHR_{ext} estimation method is subject to several limitations. First, without real-time VOC measurements, OHR_{ext} cannot be determined for all relevant gas-phase emissions. The Additionally, since particles and gases are added simultaneously, decoupling particle-phase formation of CO, gas-phase formation of CO, and OH-driven CO oxidation remains challenging. Future work will focus on determining the individual contributions of each of these mechanisms to better constrain OHR_{ext} during biomass burning experiments.

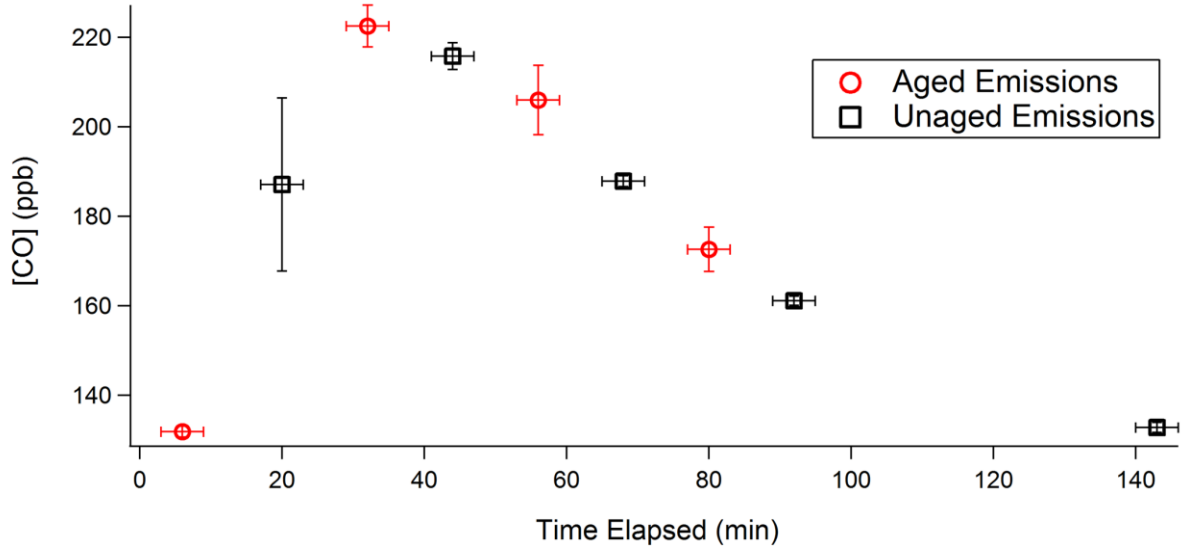

Figure S4: CO concentrations for aged and unaged leaf BBOA. The heat pulse began at time elapsed = 0.

S2.3 O_3 Measurements

To determine the extent of O_3 formation in the PAM reactor relative to externally generated O_3 concentrations, O_3 was measured with and without the PAM UV lamps on. These measurements were taken without any aerosol added to the reactor. After 15 minutes, O_3 measurements were averaged over a period of 5 minutes. Results are provided in Table S1.

These measurements were used with the Oxidation Flow Reactor Exposure Estimator version 2.3 (available for download at http://sites.google.com/site/pamwiki/hardware/estimation-equations; Peng et al., 2015) to obtain a more precise estimate of equivalent atmospheric aging. With these O_3 measurements and an OHR_{ext} of 2.2 s^{-1} (assumed based on CO measurements), we calculate an upper OH_{exp} limit of 0.3 ppm for the low-mid level of oxidation and 1.7 ppm for the highest level of oxidation. These values are used in conjunction with offline SO_2 calibrations to provide a range of equivalent aging times in Table 1.

Table S1. Internally produced PAM O_3 measurements, along with OH_{exp}, equivalent aging times, and PAM operating condition types (e.g. "safer" or "riskier") calculated using the Oxidation Flow Reactor Exposure Estimator version 2.3, available for download at http://sites.google.com/site/pamwiki/hardware/estimation-equations (Peng et al., 2015). Calculations were performed using the OFR185 portion of the spreadsheet assuming a reactor residence time of 78 s, an RH of 30%, and a maximum OHR_{ext} of 2.2 s^{-1}.

	O_3 (ppm)	OH_{exp} (molec cm^{-3} s)	Equiv. Aging (days)	Condition Type
Low-mid	0.3	1.7×10^{11}	1	Safer
High	1.7	7.7×10^{11}	6	Safer

Section S3: SMPS Measurements

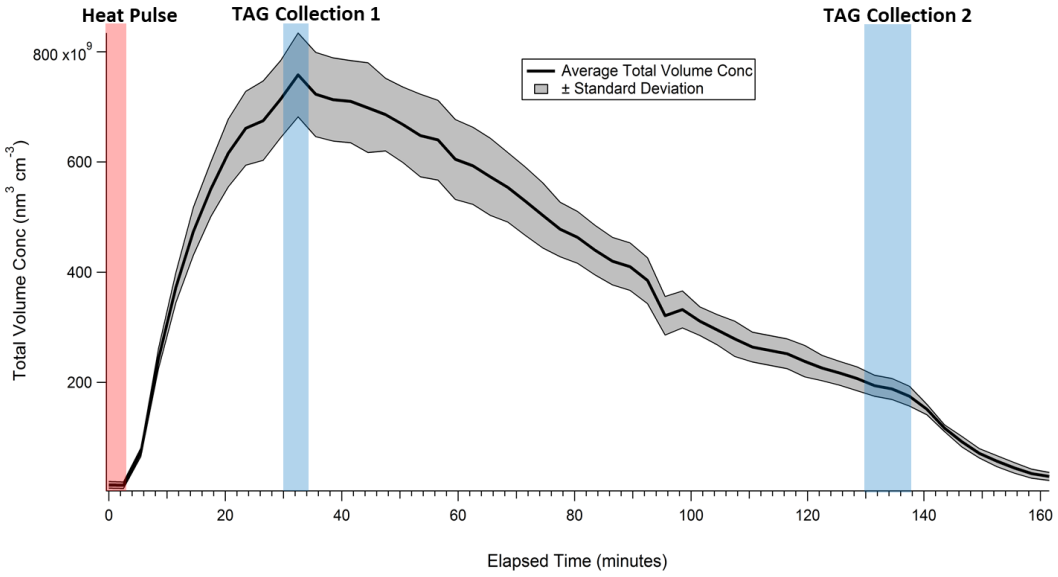

Figure S5. SMPS total volume concentration ($nm^3\ cm^{-3}$) over time for oak heartwood PM_1 at 1-3 days of equivalent aging, presented as an average of triplicate measurements (bold black trace) ± one standard deviation (gray shaded region). The heat pulse occurred during the period encompassed by the red shaded region, beginning at elapsed time = 0 minutes. All TAG data presented in this work were collected for a duration of 4 minutes beginning 30 minutes after the start of the heat pulse (blue shaded region, "TAG Collection 1"). Additional sample collections (e.g. blue shaded region, "TAG Collection 2"; other subsequent collections not shown) were also obtained to evaluate the cleanliness of the emissions and combustion chamber.

Table S2. Maximum SMPS volume concentrations ($C_{SMPS,V} \times 10^{-9}$, $nm^3\ cm^{-3}$) at each level of oxidative aging, presented as an average of triplicate measurements ± one standard deviation.

	Equivalent Aging Time (days)		
Fuel Type	**0**	**1-3**	**6-10**
Leaf	314 ± 79	211 ± 41	179 ± 28
Wood	607 ± 45	814 ± 6	791 ± 38

Section S4: AMS Chemical Characterization

In this section, we characterize the chemical properties of lab-generated heartwood and leaf BBOA using AMS data and compare the results to those obtained in previous studies.

Figure S6 gives the average mass spectrum for each fuel type at each photochemical aging condition. For both fuels, both *m/z* 28 (N_2^+ and CO^+) and *m/z* 44 (CO_2^+) increase in abundance when aged 10 days, consistent with an increase in oxidized OA observed in previous studies with various fuels (Cubison et al., 2011; Ortega et al., 2013). Notably, in the heartwood BBOA, the *m/z* 43 signal decreases overall with oxidation, while in the leaf BBOA, *m/z* 43 exhibits an increase. Since AMS total organics mass concentrations remain approximately consistent between OA aged 0 days and 10 days (Figure S7 and Table S3), this trend could signal depletion of primary products (as supported by TAG measurements) along with increased formation of less-oxidized organics (e.g. $C_2H_3O^+$) with photochemical aging. Ortega et al. observed a similar trend in *m/z* 43 in aged turkey oak BBOA after combusting 0.401 kg biomass in a 3000 m^3 chamber under flaming conditions (Ortega et al., 2013).

Van Krevelen plots for heartwood and leaf BBOA are provided in Figure S8. For heartwood BBOA, the data exhibit a trend down and to the right, indicating an increase in oxidized material with photochemical aging. By contrast, no clear trend is observed for oak leaf BBOA. Potential differences in oxidation mechanisms between the two types of BBOA are discussed further in the main text.

In general, H/C and O/C ratios are within ranges typical for smoldering oak BBOA (Ortega et al., 2013; Reece et al., 2017). However, some key discrepancies are observed in our data that may be attributed to differences in combustion techniques. For example, Ortega et al. report typical H/C values between 1.4 and 1.8 for unaged turkey oak BBOA produced with flaming combustion, while we observe H/C ratios in the range of 1.5 to 3. Similarly, in their average AMS H/C and O/C measurements for aged and unaged red oak (*Q. robur*) BBOA generated in three different types of cookstoves, Reece et al. obtain typical H/C values between 0.4 and 1.5. Notably, Reece et al. found that the open fire style cookstove exhibited a higher H/C compared to the other two cookstove models, which both utilized more efficient combustion techniques (Reece et al., 2017). From AMS measurements of laboratory-generated BBOA from three different tree species, Weimer et al. obtained mass spectra dominated by *m/z* 44 and resembling fulvic acid, particularly from primary smoldering BBOA and from SOA. While their findings suggest that smoldering conditions should produce highly oxidized primary aerosol (i.e. with reduced H/C and increased O/C), it should be noted that their combustion technique differs fundamentally from the method presented in this work in that their smoldering stage follows a period of flaming combustion, allowing more rapid devolatilization of hydrocarbons that might otherwise exist in the particle phase. Therefore, we expect the BBOA produced using our method to be less oxidized than that produced by their smoldering technique.

The results from these studies, in conjunction with the data reported here, demonstrate the influence of combustion conditions on chemical characterization of aged and unaged BBOA.

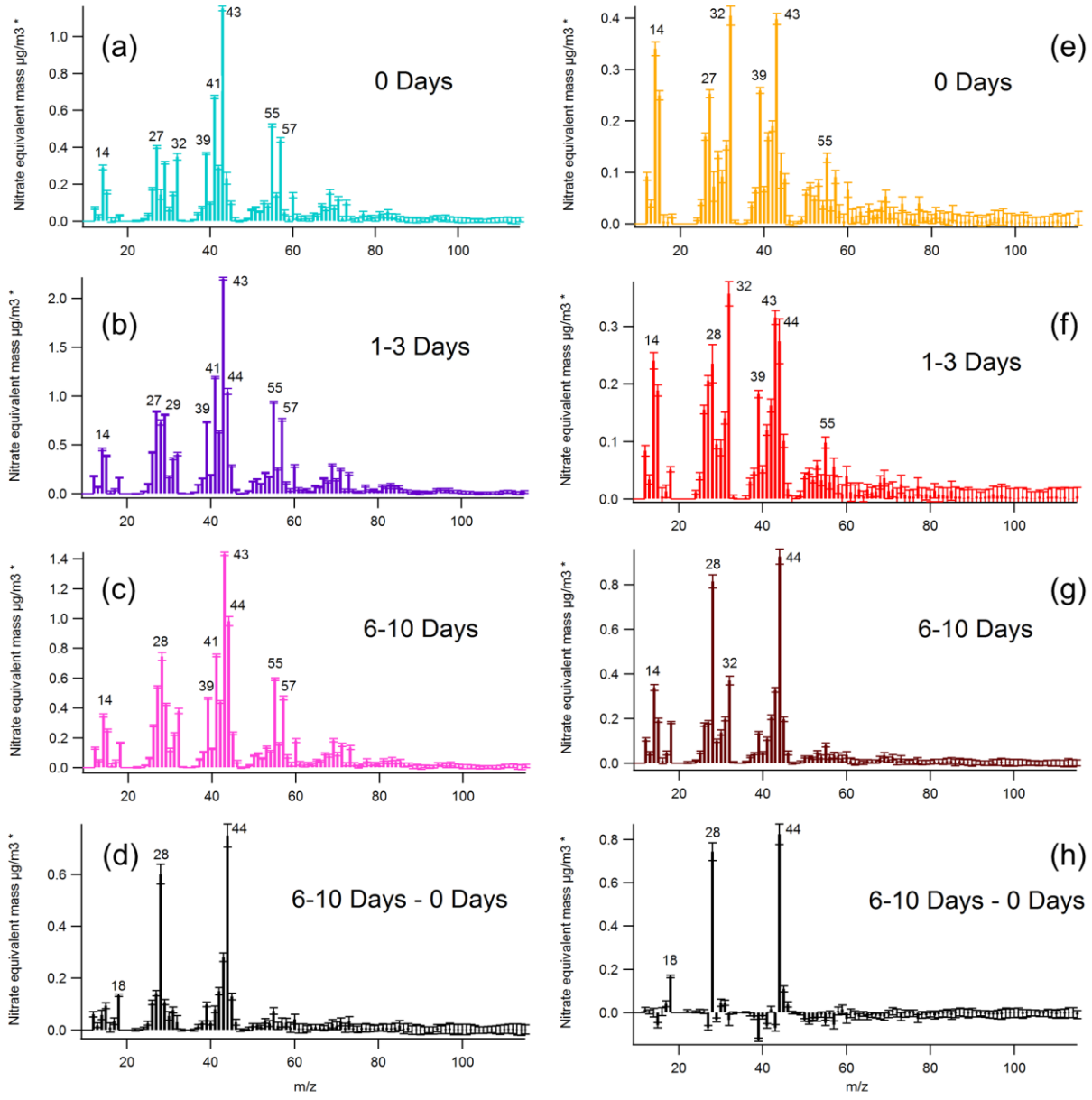

Figure S6. Average AMS mass spectra for leaf and heartwood fuels under each oxidation condition: (a) leaf BBOA, unaged ("0 days"); (b) leaf BBOA, aged 1-3 days; (c) leaf BBOA, aged 6-10 days; (d) leaf BBOA, difference between particles aged 10 days and unaged particles; (e) heartwood BBOA, unaged ("0 days"); (f) heartwood BBOA, aged 1-3 days; (g) heartwood BBOA, aged 6-10 days; (h) heartwood BBOA, difference between particles aged 6-10 days and unaged particles.

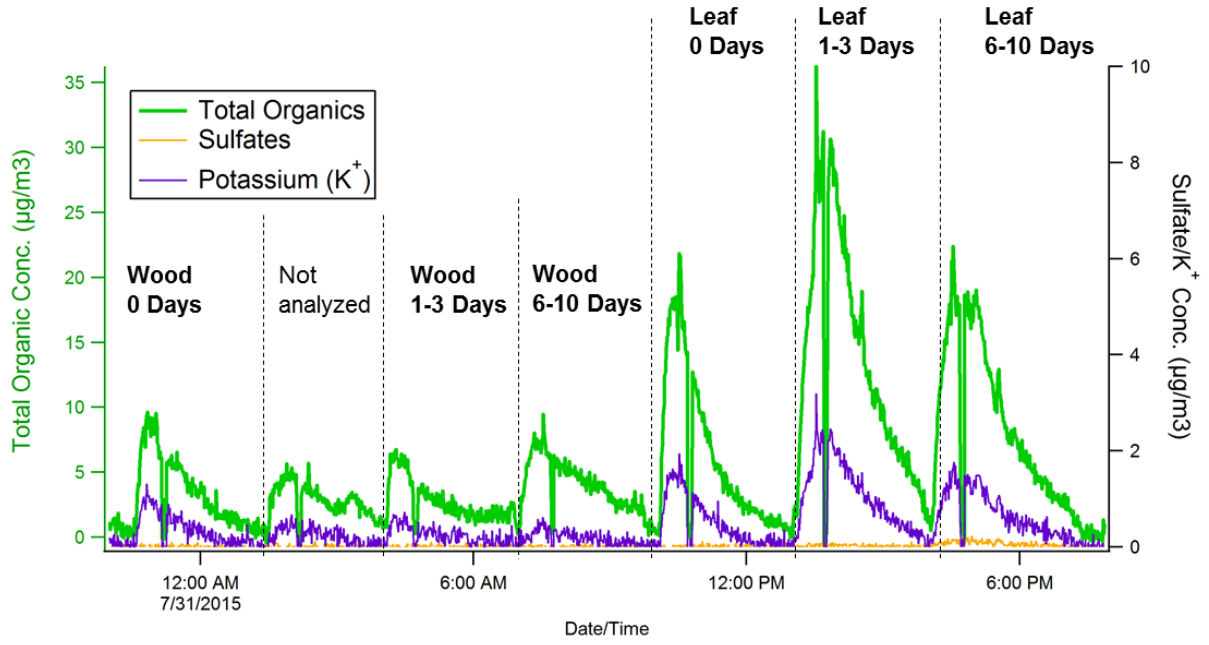

Figure S7: Total organic, sulfate, and potassium (K^+) concentrations measured by the AMS. Due to an error in the burn procedure, the run labeled "not analyzed" is not included in this analysis.

Table S3. Average peak AMS total organic concentrations (C_{Org}, µg m^{-3}) and corresponding SMPS volume concentrations ($C_{SMPS,V} \times 10^9$, nm^3 cm^{-3}) at each level of oxidative aging.

	Equivalent Aging Time (days)					
	0		**1-3**		**6-10**	
Fuel Type	C_{Org}, (µg m^{-3})	$C_{SMPS,V} \times 10^9$ (nm^3 cm^{-3})	C_{Org}, (µg m^{-3})	$C_{SMPS,V} \times 10^9$ (nm^3 cm^{-3})	C_{Org}, (µg m^{-3})	$C_{SMPS,V} \times 10^9$ (nm^3 cm^{-3})
Leaf	17.8	157	29.2	163	19.0	135
Heartwood	8.56	259	6.20	254	7.19	279

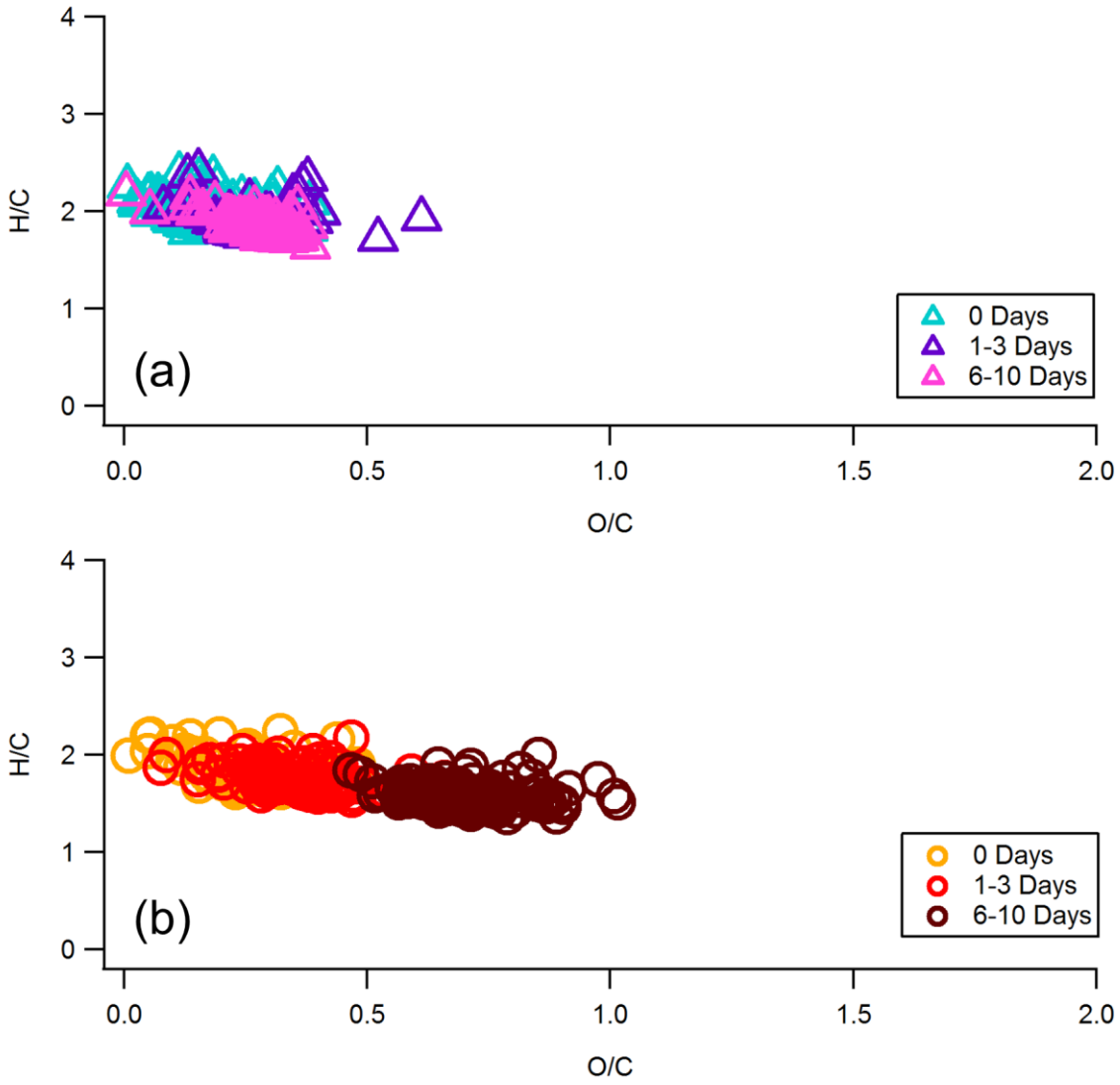

Figure S8: Van Krevelen diagrams with AMS-obtained H/C and O/C ratios for (a) leaf BBOA and (b) heartwood BBOA. To minimize noise, AMS data is plotted only for points where sufficient total organic concentrations were achieved.

Section S5: TAG Supplemental Results

Table S4. Dot products of mass spectral unit vectors obtained from TAG chromatograms collected using the same amount of fuel mass. These values were determined by taking the dot products between each mass spectral vector within a given fuel and oxidation condition, then averaging each dot product. A dot product of 1 signifies a perfect mass spectral match, and a dot product of 0 indicates a complete mismatch (Stein and Scott, 1994).

	Equivalent Aging Time (days)		
Fuel Type	**0**	**1-3**	**6-10**
Leaf	0.980 ± 0.008	0.948 ± 0.03	0.898 ± 0.07
Heartwood	0.995 ± 0.002	0.997 ± 0.002	0.997 ± 0.002

Table S5. Selected compounds of interest identified in oak leaf BBOA TAG chromatograms. Common compound names were used in this work where appropriate and are provided in parentheses. Estimated subcooled liquid vapor pressures (p_L°), saturation concentrations (C^*) and corresponding volatility classifications are also provided. Compounds are classified as intermediately volatile, semivolatile, low volatility, or extremely low volatility organic compounds (I-, S-, L-, ELVOCs, respectively) based on the compound's $\log_{10}(C^*)$ value and criteria outlined in previous literature.

Structure	Compound Name	Certainty of ID[a]	Molecular Formula	Predicted p_L^o at 25°C (Pa)[b]	$\log_{10}(C^*)$ (μg m^{-3})[c]	Volatility Classification[d]
1	1,6-anhydro-β-glucopyranose (levoglucosan)	A	$C_6H_{10}O_5$	2.41×10^{-5}	0.31	SVOC
2	Quinic Acid	A	$C_7H_{12}O_6$	2.11×10^{-7}	-1.67	LVOC
3	Mannose	B	$C_{16}H_{12}O_6$	3.45×10^{-11}	-5.49	ELVOC
4	Octadecanoic Acid	B	$C_{18}H_{36}O_2$	1.14×10^{-3}	2.23	SVOC
5	Tricosane (C_{23} alkane)	A	$C_{23}H_{48}$	1.65×10^{-3}	2.45	SVOC
6	Tetracosene (C_{24} alkene)	D	$C_{24}H_{48}$	1.08×10^{-3}	2.28	SVOC
7	Pentacosane (C_{25} alkane)	A	$C_{25}H_{52}$	3.55×10^{-4}	1.82	SVOC
8	Tetracosanal (C_{24} aldehyde)	D	$C_{24}H_{48}O$	7.87×10^{-4}	2.16	SVOC
9	Tetracosanol (C_{24} alcohol)	D	$C_{24}H_{50}O$	9.79×10^{-6}	0.260	SVOC
10	Hexacosanal (C_{26} aldehyde)	D	$C_{26}H_{52}O$	2.47×10^{-4}	1.69	SVOC
11	Nonacosane (C_{29} alkane)	A	$C_{29}H_{60}$	1.96×10^{-5}	0.623	SVOC
12	Octacosanal (C_{28} aldehyde)	D	$C_{28}H_{56}O$	8.24×10^{-5}	1.25	SVOC
13	Triacontanal (C_{30} aldehyde)	D	$C_{30}H_{60}O$	2.92×10^{-5}	0.825	SVOC
14	D:A-Friedoolean-6-ene	B	$C_{30}H_{50}$	8.20×10^{-6}	0.247	SVOC
15	Dotriacontanal (C_{32} aldehyde)	D	$C_{32}H_{64}O$	1.10×10^{-5}	0.426	SVOC
16	Friedelan-3-one **(**Friedelin**)**	B	$C_{30}H_{50}O$	3.81×10^{-7}	-1.07	LVOC

[a] Identification certainty ("Certainty of ID") was classified for each compound according to the following criteria: (A) the compound was positively identified based on external standard injections; (B) the compound was identified based on a high match quality (MQ > 75%) using available mass spectral libraries; (C) the compound was identified based on a low-to-moderate match quality (MQ < 75%) using available mass spectral libraries; and (D) no adequate mass spectral library match was available for the compound, so the compound structure was determined by retention time and manually evaluating possible fragmentation patterns.

[b] Vapor pressures at 25°C were predicted using the Advanced Chemistry Development (ACD/Labs) Software V11.02 (© 1994-2017 ACD/Labs) through the SciFinder website (ACD/Labs, 2017).

[c] $\log_{10}(C^*)$ values calculated using methods outlined in Pankow, et al. (Pankow, 1994). An activity coefficient of 1.3 was assumed based on a typical estimated BBOA activity coefficient of 1.3 (Donahue et al., 2011).

[d] Defined using criteria set forth in previous work (Donahue et al., 2011, 2012).

Table S5, cont'd. Selected compounds of interest identified in oak wood BBOA TAG chromatograms. Common compound names were used in this work where appropriate and are provided in parentheses. Estimated subcooled liquid vapor pressures (p_L°), saturation concentrations (C^*) and corresponding volatility classifications are also provided. Compounds are classified as intermediately volatile, semivolatile, low volatility, or extremely low volatility organic compounds (I-, S-, L-, ELVOCs, respectively) based on the compound's $\log_{10}(C^*)$ value and criteria outlined in previous literature.

Structure	Compound Name	Certainty of ID[a]	Molecular Formula	Predicted p_L^o at 25°C (Pa)[b]	$\log_{10}(C^*)$ ($\mu g\ m^{-3}$)[c]	Volatility Classification[d]
17	2,6-dimethoxy-phenol (syringol)	B	$C_8H_{10}O_3$	7.88×10^{-1}	4.80	IVOC
18	4-hydroxy-3-methoxy-benzaldehyde (vanillin)	B	$C_8H_8O_3$	2.59×10^{-1}	4.31	IVOC
19	4-(1,2-propadienyl)-guaiacol	C	$C_{10}H_{10}O_2$	1.55×10^{-1}	4.12	IVOC
20	1,6-anhydro-β-glucopyranose (levoglucosan)	A	$C_6H_{10}O_5$	2.41×10^{-5}	0.31	SVOC
21	galacto-heptulose	C	$C_7H_{14}O_7$	2.77×10^{-16}	-10.51	ELVOC
22	1,6-anhydro-α-d-galactofuranose	C	$C_6H_{10}O_5$	1.49×10^{-6}	-0.896	LVOC
23	methyl-β-D-glucopyranoside	C	$C_7H_{14}O_6$	1.53×10^{-5}	0.19	SVOC
24	n-acetyl-d-galactosamine	C	$C_8H_{15}NO_6$	9.49×10^{-17}	-10.96	ELVOC
25	2,6-di-methoxy-4-vinyl-phenol (4-vinyl-syringol)	B	$C_{10}H_{12}O_3$	2.17×10^{-1}	4.31	IVOC
26	4-hydroxy-3,5-dimethoxy-benzaldehyde (syringaldehyde)	B	$C_9H_{10}O_4$	2.01×10^{-2}	3.28	IVOC
27	2,6-dimethoxy-4-(1-propynyl)-phenol	C	$C_{11}H_{12}O_3$	1.19×10^{-2}	3.08	IVOC
28	1-(4-hydroxy-3,5-dimethoxyphenyl)-ethanone (acetosyringone)	B	$C_{10}H_{12}O_4$	8.65×10^{-3}	2.95	IVOC
29	3-(4-hydroxy-3-methoxyphenyl)prop-2-enal (coniferaldehyde)	B	$C_{10}H_{10}O_3$	6.51×10^{-3}	2.78	IVOC
30	4-(2-oxopropyl)-syringol (syringyl acetone)	B	$C_{11}H_{14}O_4$	5.99×10^{-3}	2.82	IVOC
31	4-hydroxy-3,5-dimethoxycinnamaldehyde (sinapaldehyde)	B	$C_{11}H_{12}O_4$	6.04×10^{-4}	1.82	SVOC

[a] Identification certainty ("Certainty of ID") was classified for each compound according to the following criteria: (A) the compound was positively identified based on external standard injections; (B) the compound was identified based on a high match quality (MQ > 75%) using available mass spectral libraries; (C) the compound was identified based on a low-to-moderate match quality (MQ < 75%) using available mass spectral libraries; and (D) no adequate mass spectral library match was available for the compound, so the compound structure was determined by retention time and manually evaluating possible fragmentation patterns.

[b] Vapor pressures at 25°C were predicted using the Advanced Chemistry Development (ACD/Labs) Software V11.02 (© 1994-2017 ACD/Labs) through the SciFinder website (ACD/Labs, 2017).

[c] $\log_{10}(C^*)$ values calculated using methods outlined in Pankow, et al. (Pankow, 1994). An activity coefficient of 1.3 was assumed based on a typical estimated BBOA activity coefficient of 1.3 (Donahue et al., 2011).

[d] Defined using criteria set forth in previous work (Donahue et al., 2011, 2012).

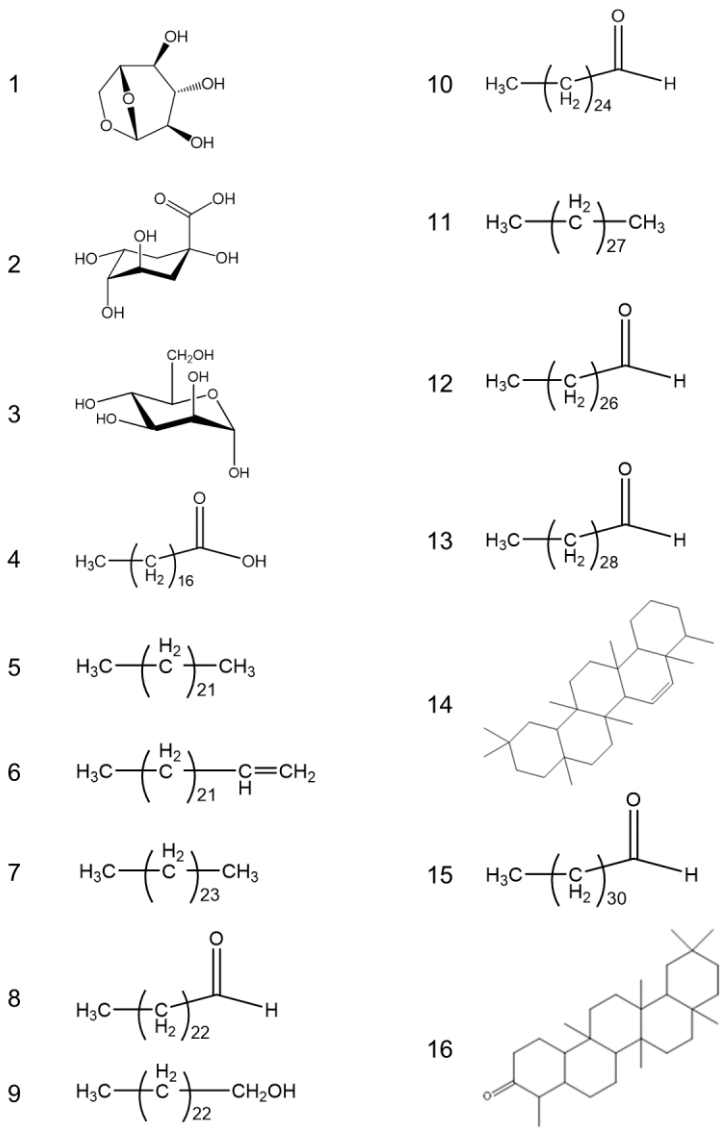

Figure S9: Structures identified in oak leaf BBOA TAG chromatograms. Corresponding compound names are provided in Table S5.

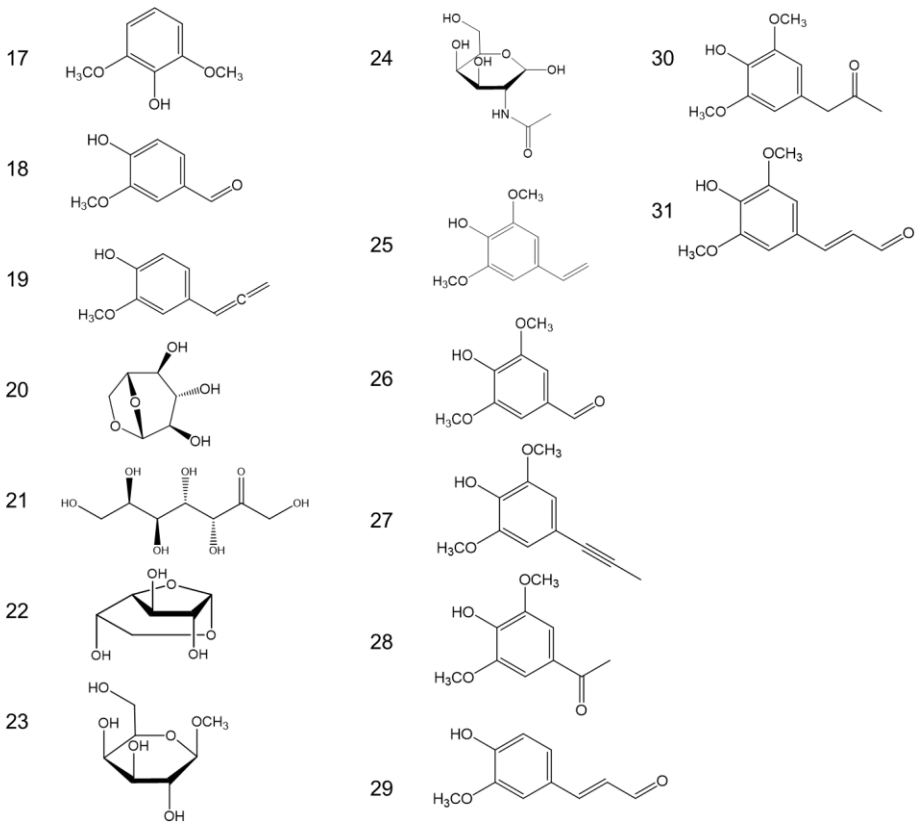

Figure S9, cont'd: Structures identified in oak heartwood BBOA TAG chromatograms. Corresponding compound names are provided in Table S5.

Table S6. Raw SIC integrations, reported as a triplicate average ± one standard deviation (%), for each compound reported in Table S4 at each equivalent aging time.

Compound	**Ion Integrated**	**Equivalent Aging Time (days)**		
		0	**1-3**	**6-10**
1,6-anhydro-β-glucopyranose (levoglucosan)	60	1.81×10^{6} ± 81%	2.05×10^{5} ± 105%	3.07×10^{4} ± 83%
Quinic Acid	60	1.10×10^{7} ± 58%	1.85×10^{6} ± 95%	5.64×10^{5} ± 100%
Mannose	60	1.25×10^{6} ± 69%	5.07×10^{4} ± 86%	3.01×10^{3} ± 73%
Octadecanoic Acid	60	1.53×10^{5} ± 84%	9.66×10^{3} ± 44%	0*
Tricosane (C_{23} alkane)	57	1.44×10^{6} ± 40%	5.86×10^{5} ± 18%	3.33×10^{5} ± 27%
Pentacosane (C_{25} alkane)	57	2.91×10^{6} ± 50%	1.06×10^{6} ± 22%	4.37×10^{5} ± 36%
Tetracosanal (C_{24} aldehyde)	82	5.68×10^{6} ± 28%	2.83×10^{6} ± 24%	6.62×10^{5} ± 133%
Tetracosanol (C_{24} alcohol)	97	2.53×10^{7} ± 41%	7.15×10^{6} ± 52%	1.67×10^{6} ± 91%
Hexacosanal (C_{26} aldehyde)	82	4.85×10^{6} ± 52%	8.17×10^{5} ± 52%	1.24×10^{5} ± 100%
Nonacosane (C_{29} alkane)	57	5.24×10^{6} ± 47%	2.00×10^{6} ± 23%	7.54×10^{5} ± 44%
Octacosanal (C_{28} aldehyde)	82	5.29×10^{6} ± 60%	4.70×10^{5} ± 74%	3.71×10^{4} ± 105%
Triacontanal (C_{30} aldehyde)	82	2.73×10^{6} ± 74%	7.94×10^{4} ± 76%	3.97×10^{3} ± 141%
Dotriacontanal (C_{32} aldehyde)	82	6.25×10^{5} ± 81%	0*	0*
D:A-Friedoolean-6-ene	95	1.58×10^{6} ± 38%	6.26×10^{5} ± 30%	2.20×10^{5} ± 60%
Friedelan-3-one **(**Friedelin**)**	95	1.69×10^{6} ± 53%	3.16×10^{5} ± 52%	7.34×10^{4} ± 75%

*Signal not present above noise in any of the triplicate chromatograms.

Table S6, cont'd. Raw SIC integrations, reported as a triplicate average ± one standard deviation (%), for each compound reported in Table S5 at each equivalent aging time.

Compound	Ion Integrated	Equivalent Aging Time (days) 0	1-3	6-10
2,6-dimethoxy-phenol (syringol)	154	1.20×10^{6} ± 10%	3.01×10^{6} ± 6%	1.34×10^{6} ± 5%
4-hydroxy-3-methoxy-benzaldehyde (vanillin)	152	5.08×10^{5} ± 22%	6.11×10^{6} ± 5%	1.38×10^{6} ± 16%
4-(1,2-propadienyl)-guaiacol	162	1.99×10^{6} ± 12%	1.51×10^{5} ± 9%	2.08×10^{4} ± 12%
1,6-anhydro-β-glucopyranose (levoglucosan)	60	1.89×10^{7} ± 6%	2.42×10^{7} ± 11%	4.20×10^{6} ± 12%
galacto-heptulose	60	5.59×10^{5} ± 28%	1.07×10^{6} ± 22%	1.55×10^{5} ± 4%
1,6-anhydro-α-d-galactofuranose	60	7.46×10^{4} ± 10%	1.08×10^{5} ± 14%	0*
methyl-β-D-glucopyranoside	60	7.94×10^{4} ± 7%	1.06×10^{5} ± 2%	2.12×10^{4} ± 0%
n-acetyl-d-galactosamine	60	1.52×10^{5} ± 11%	2.05×10^{5} ± 7%	5.02×10^{4} ± 5%
2,6-di-methoxy-4-vinyl-phenol (4-vinyl-syringol)	180	9.87×10^{5} ± 4%	7.65×10^{5} ± 2%	3.02×10^{5} ± 9%
4-hydroxy-3,5-dimethoxy-benzaldehyde (syringaldehyde)	182	2.92×10^{6} ± 14%	8.38×10^{6} ± 2%	2.70×10^{6} ± 13%
2,6-dimethoxy-4-(1-propynyl)-phenol	192	2.29×10^{6} ± 11%	9.35×10^{4} ± 10%	1.24×10^{4} ± 21%
1-(4-hydroxy-3,5-dimethoxyphenyl)-ethanone (acetosyringone)	181	1.89×10^{6} ± 10%	1.37×10^{6} ± 2%	5.59×10^{5} ± 9%
3-(4-hydroxy-3-methoxyphenyl)prop-2-enal (coniferaldehyde)	178	2.23×10^{6} ± 26%	8.74×10^{5} ± 6%	8.90×10^{4} ± 23%
4-(2-oxopropyl)-syringol (syringyl acetone)	210	2.61×10^{6} ± 14%	1.36×10^{6} ± 6%	1.66×10^{5} ± 22%
4-hydroxy-2-methoxycinnamaldehyde (sinapaldehyde)	208	2.00×10^{7} ± 4%	8.04×10^{6} ± 1%	1.47×10^{6} ± 13%

*Signal not present above noise in any of the triplicate chromatograms.

S5.1 Method: Oak leaf solvent extractions

The solvent extraction method used to extract leaf wax components was adapted from a previously published method (Gulz and Boor, 1992). A 52.9 ± 0.5 mg leaf sample was gently broken into roughly centimeter-wide pieces and added to 2 mL of a 2:1:1 mixture of chloroform, acetone, and methanol. The leaf sample was submerged in the solvent mixture for one minute under gentle agitation by hand. The leaf was then removed for one minute and submerged again for one minute. Solid leaf components were decanted from the extraction prior to TAG analysis. A 3 µL aliquot of the extraction was injected onto the TAG CTD cell through its standard injection port (Kreisberg et al., 2009), desorbed, separated, and analyzed using the previously described TAG thermal desorption and GC oven programs.

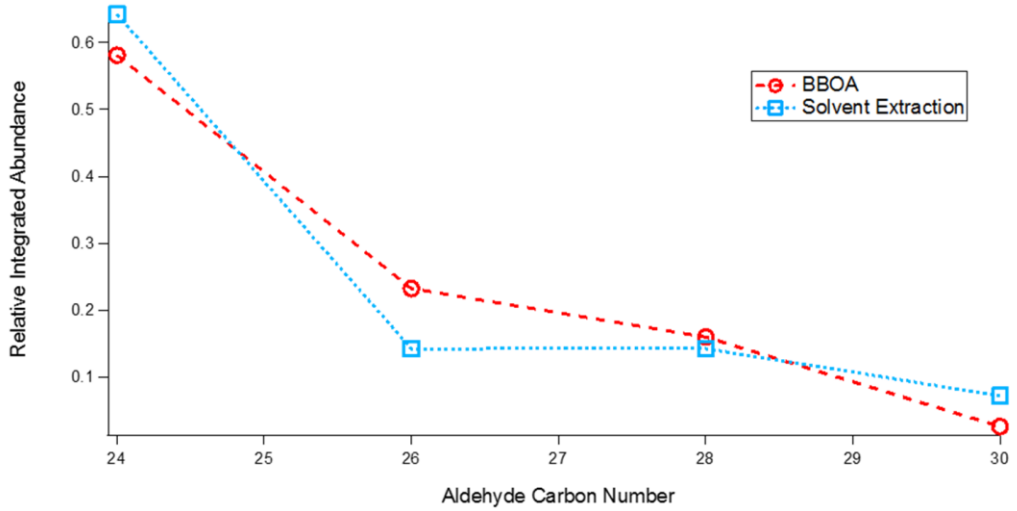

Figure S10. Relative integrated abundances for four different aldehydes measured in a TAG leaf BBOA chromatogram (0 days of equivalent aging) and a solvent extraction chromatogram. Each point corresponds to the integrated *m/z* 82 abundance normalized to the sum of the integrated *m/z* 82 abundances over the four different aldehydes within the chromatogram.

Table S7. Particle-phase fractions (ξ_i) for several compounds obtained using calculated saturation concentrations (C_i*, µg m-3; Table S5) and AMS total organic concentrations (C_{OA}, Table S3). These values were calculated according to equation 1 of the main text (Donahue et al., 2006).

Fuel Type	Structure	Compound Name	Equivalent Aging Time (days)		
			0	1-3	6-10
Leaf	1	levoglucosan	0.897	0.934	0.902
Heartwood	17	syringol	1.34×10^{-4}	9.73×10^{-5}	1.13×10^{-4}
	18	vanillin	4.15×10^{-4}	3.00×10^{-4}	3.48×10^{-4}
	20	levoglucosan	0.807	0.751	0.778
	26	syringaldehyde	0.00443	0.00321	0.00372

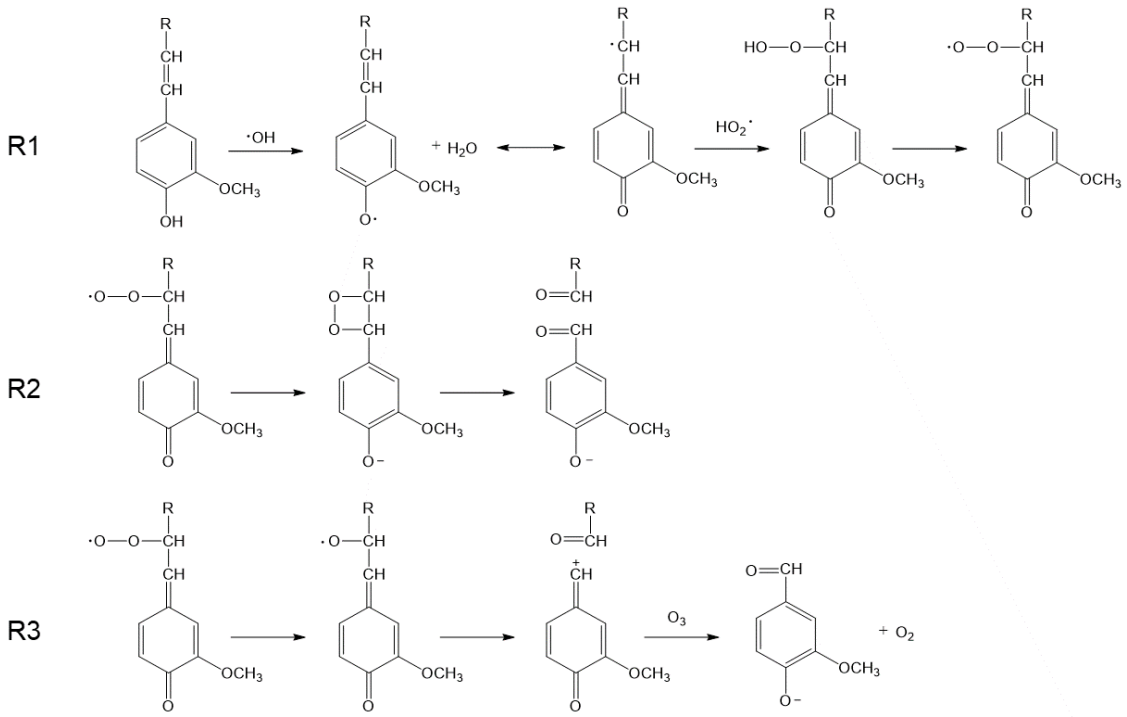

Figure S11. One possible mechanism for the formation of vanillin from larger lignin decomposition products within the PAM reactor. In the first stage (**R1**), a peroxy radical intermediate is formed following OH-driven hydrogen abstraction from the phenolic substituent, rearrangement, and HO_2 radical addition to the beta carbon. In the second stage (**R2**), the radical intermediate undergoes an intramolecular nucleophilic attack, causing breakage of the C_α-C_β bond and resulting in formation of two distinct aldehydes. This mechanism assumes sufficiently high concentrations of the HO_2 radical are present within the reactor. A third reaction sequence (**R3**) could also proceed after R1 following loss of an oxygen from the peroxy radical through reaction with either HO_2 or another peroxy radical (RO_2; Ziemann and Atkinson, 2012). Both R1 and R2 were adapted from the alkaline oxygen delignification mechanism described by Wong et al. (Wong et al., 2010).

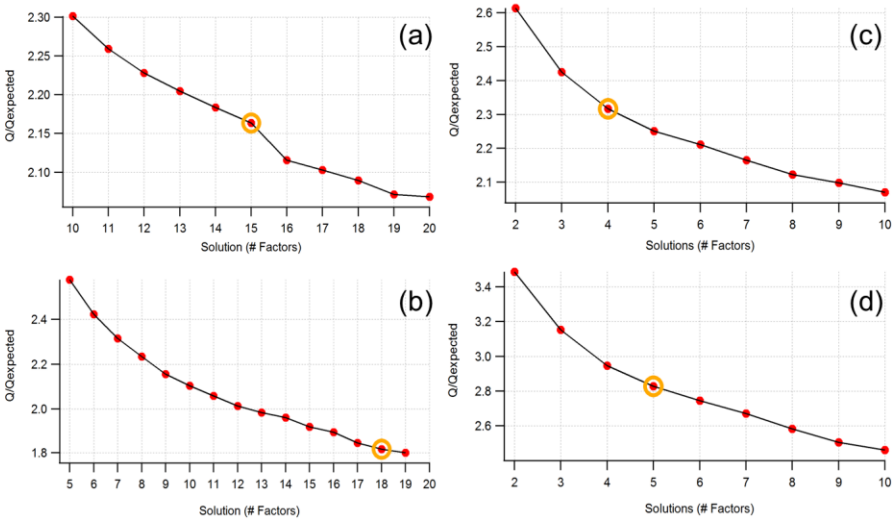

Figure S12. Q/Q_{exp} as a function of factor number, where the orange circle indicates the number of factors in the chosen solution for PMF calculations on: **(a)** oak leaf compound window; **(b)** oak heartwood compound window; **(c)** oak leaf decomposition window; **(d)** oak heartwood decomposition window.

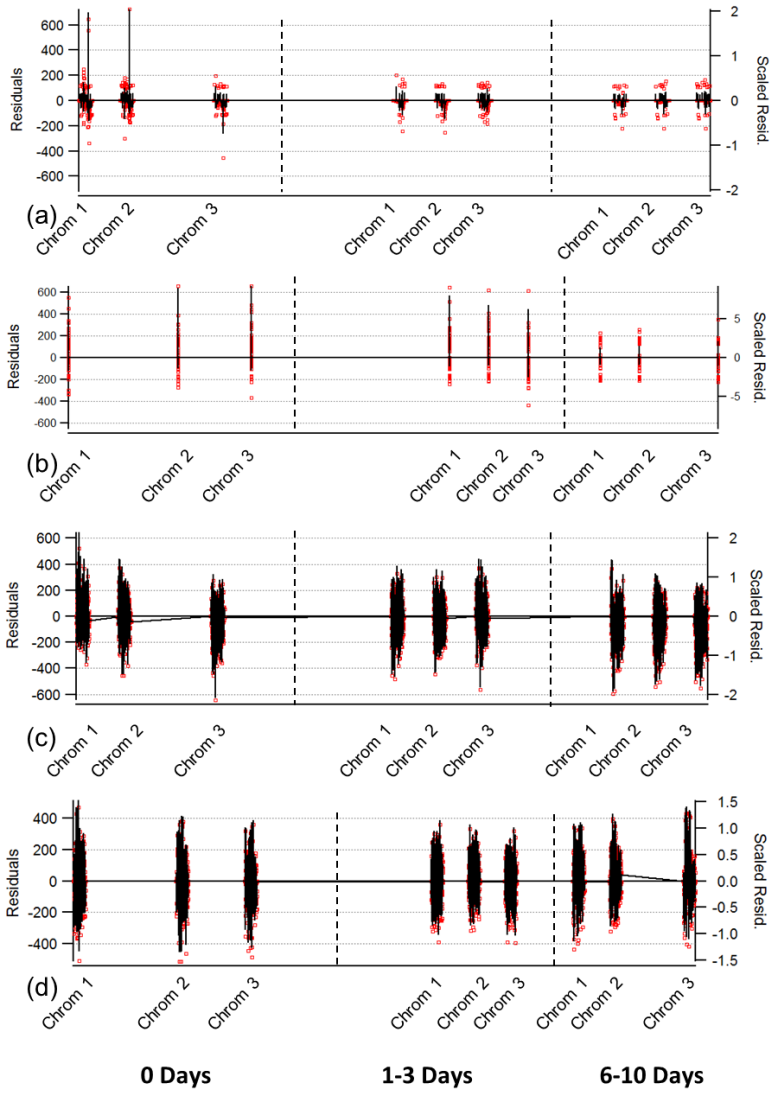

Figure S13. Residuals (black lines) and scaled residuals (red dots) from PMF calculations on: **(a)** oak leaf compound window; **(b)** oak heartwood compound window; **(c)** oak leaf decomposition window; **(d)** oak heartwood decomposition window.

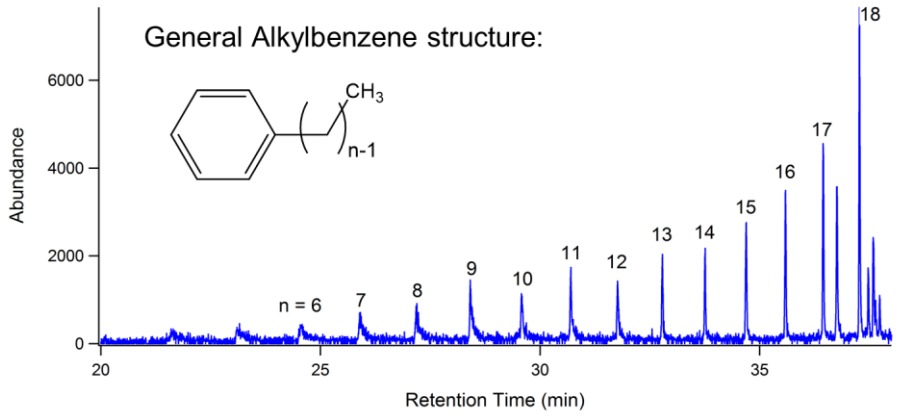

Figure S14. *m/z* 92 single ion chromatogram (SIC) from TAG analysis of oak leaf extract showing a series of alkylbenzenes. The number above each peak denotes the number of carbons (*n*) present in the alkyl chain (e.g. *n* = 9 corresponds to nonyl-benzene).

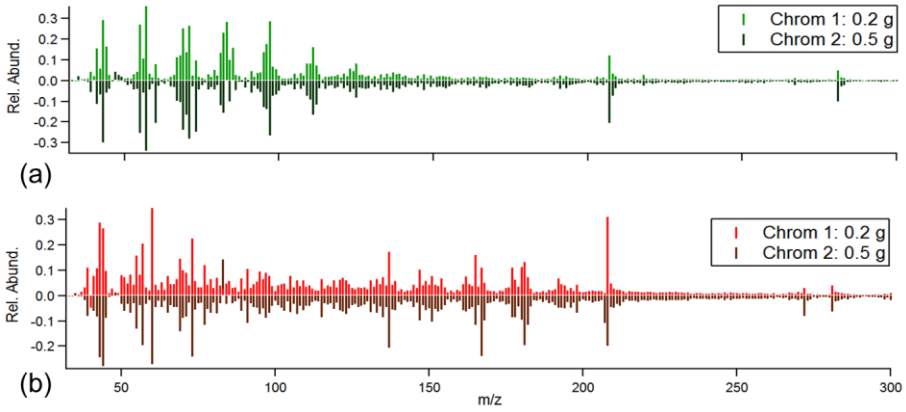

Figure S15. Summed mass spectra for unaged BBOA chromatograms obtained using 0.2 g ("Chrom 1") and 0.5 g ("Chrom 2") of: **(a)** oak leaf, and **(b)** oak heartwood. Each mass spectrum was obtained from the chromatogram by subtracting an appropriate system blank, summing all ions across the full chromatogram, and converting the resulting mass spectrum vector to a unit vector per the technique outlined in Stein and Scott (Stein and Scott, 1994). In both plots, the "Chrom 2" unit vector is displayed with a negative relative abundance to facilitate visual comparison of the mass spectra.

Table S8. Dot products of mass spectral unit vectors obtained from TAG chromatograms collected using two different fuel masses at each equivalent aging time. A dot product of 1 signifies a perfect mass spectral match, and a dot product of 0 indicates a complete mismatch (Stein and Scott, 1994).

	Equivalent Aging Time (days)		
Fuel Type	**0**	**1-3**	**6-10**
Leaf	0.847	0.764	0.787
Heartwood	0.934	0.784	0.843

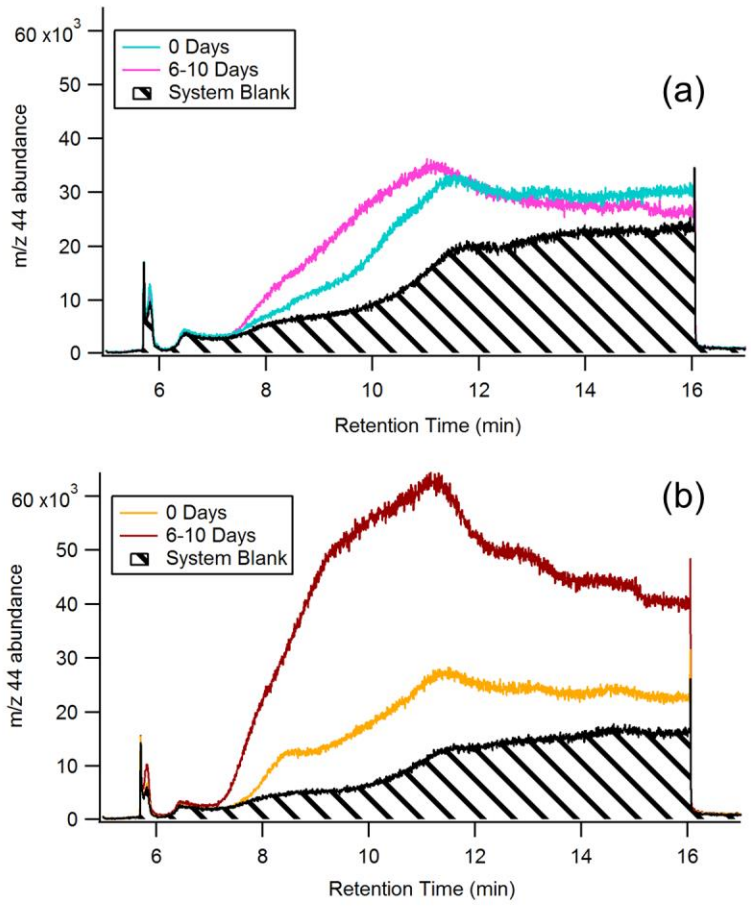

Figure S16. Example raw *m/z* 44 single ion chromatograms (SIC), with system blank *m/z* 44 SICs overlaid for comparison, obtained from TAG analysis of **(a)** oak leaf BBOA and **(b)** oak heartwood BBOA.

Table S9. Relative abundances of integrated compounds displayed in Figure 12, presented as triplicate-averaged percentages of the total compound window *m/z* 60 signal.

Fuel Type	Compound	Equivalent Aging Time (days) 0	1-3	6-10
Leaf	levoglucosan	8 ± 4%	5 ± 2%	3 ± 0%[a]
	quinic acid	61 ± 5%	44 ± 16%	49 ± 8%[a]
	mannose	5 ± 3%	1 ± 0%	0 ± 0%[a]
	octadecanoic acid	1 ± 0%	0 ± 0%	0[b]
Heartwood	methyl-β-D-glucopyranoside	0 ± 0%	0 ± 0%	0 ± 0%
	levoglucosan	82 ± 1%	82 ± 0%	71 ± 1%
	galacto-heptulose	2 ± 1%	4 ± 0%	3 ± 0%
	n-acetyl-d-galactosamine	1 ± 0%	1 ± 0%	1 ± 0%
	1,6-anhydro-α-d-galactofuranose	0 ± 0%	0 ± 0%	0[b]

[a] Signal only present above noise in two of three triplicate chromatograms; values are therefore obtained using the two chromatograms with sufficient signal.
[b] Signal not present above noise in any of the triplicate chromatograms.

Table S10. Relative abundances of triplicate-averaged total integrated compound window and decomposition window *m/z* 60 signals, presented as a percentages of the total TAG *m/z* 60 signal (compound window + decomposition window).

Fuel Type	Window	Equivalent Aging 0	1-3	6-10
Leaf	Compound	97 ± 2%	81 ± 9%	67 ± 13%
	Decomposition	3 ± 2%	19 ± 9%	33 ± 13%
Heartwood	Compound	96 ± 0%	94 ± 1%	76 ± 2%
	Decomposition	4 ± 0%	6 ± 1%	24 ± 2%

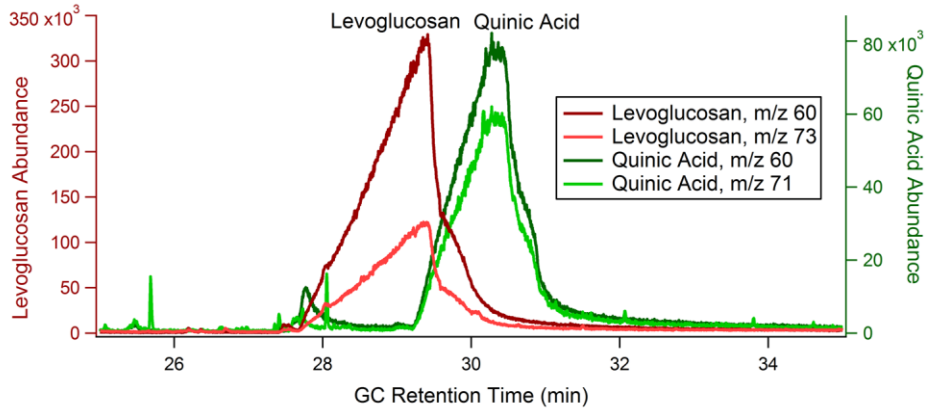

Figure S17. Results from levoglucosan (15 µg) and quinic acid (5 µg) TAG standard injections.

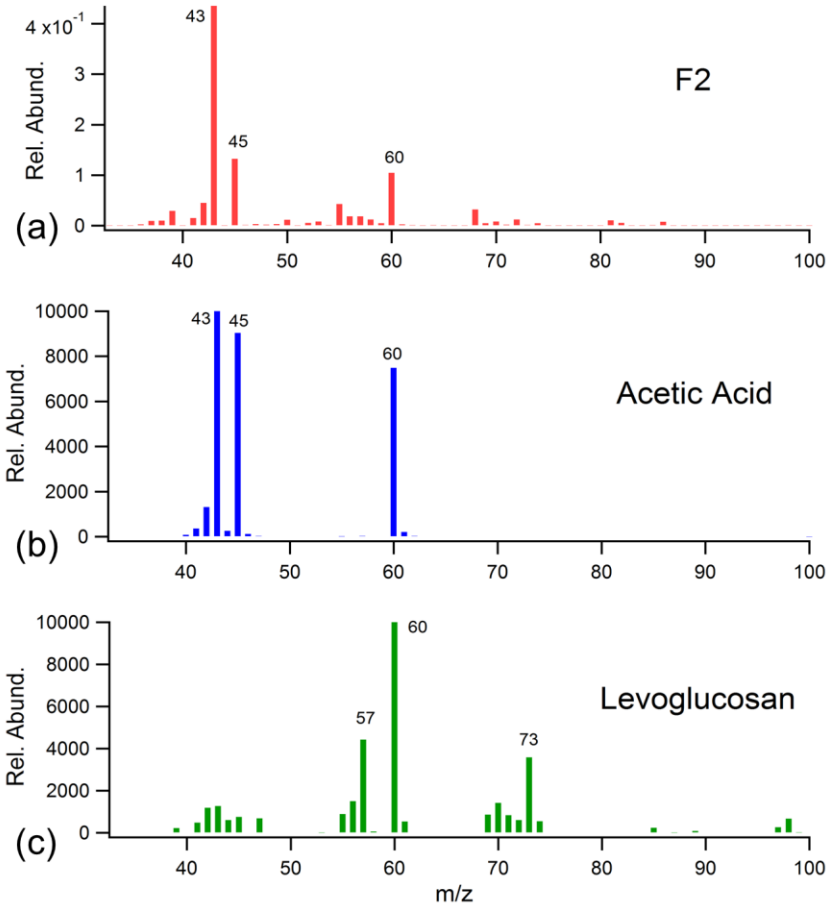

Figure S18. Electron ionization mass spectra for **(a)** Factor 2 (F2) obtained during oak wood decomposition PMF analysis (Figure 10), **(b)** Acetic acid (NIST Mass Spec Data Center), and **(c)** levoglucosan (NIST Mass Spec Data Center).

References

ACD/Labs: Advanced Chemistry Development (ACD/Labs) Software V11.02 (© 1994–2012 ACD/Labs), Retrieved from http: //www.cas.org/products/scifinder, 11 May, 2017.

Burling, I. R., Yokelson, R. J., Griffith, D. W. T., Johnson, T. J., Veres, P., Roberts, J. M., Warneke, C., Urbanski, S. P., Reardon, J., Weise, D. R., Hao, W. M. and de Gouw, J.: Laboratory measurements of trace gas emissions from biomass burning of fuel types from the southeastern and southwestern United States, Atmos Chem Phys, 10(22), 11115–11130, https://doi.org/10.5194/acp-10-11115-2010, 2010.

Cubison, M. J., Ortega, A. M., Hayes, P. L., Farmer, D. K., Day, D., Lechner, M. J., Brune, W. H., Apel, E., Diskin, G. S., Fisher, J. A., Fuelberg, H. E., Hecobian, A., Knapp, D. J., Mikoviny, T., Riemer, D., Sachse, G. W., Sessions, W., Weber, R. J., Weinheimer, A. J., Wisthaler, A. and Jimenez, J. L.: Effects of aging on organic aerosol from open biomass burning smoke in aircraft and laboratory studies, Atmos Chem Phys, 11(23), 12049–12064, https://doi.org/10.5194/acp-11-12049-2011, 2011.

Davis, D. D., Ravishankara, A. R. and Fischer, S.: SO2 oxidation via the hydroxyl radical: Atmospheric fate of HSOx radicals, Geophys. Res. Lett., 6(2), 113–116, https://doi.org/10.1029/GL006i002p00113, 1979.

Donahue, N. M., Robinson, A. L., Stanier, C. O. and Pandis, S. N.: Coupled Partitioning, Dilution, and Chemical Aging of Semivolatile Organics, Environ. Sci. Technol., 40(8), 2635–2643, https://doi.org/10.1021/es052297c, 2006.

Donahue, N. M., Epstein, S. A., Pandis, S. N. and Robinson, A. L.: A two-dimensional volatility basis set: 1. organic-aerosol mixing thermodynamics, Atmos Chem Phys, 11(7), 3303–3318, https://doi.org/10.5194/acp-11-3303-2011, 2011.

Donahue, N. M., Kroll, J. H., Pandis, S. N. and Robinson, A. L.: A two-dimensional volatility basis set – Part 2: Diagnostics of organic-aerosol evolution, Atmos Chem Phys, 12(2), 615–634, https://doi.org/10.5194/acp-12-615-2012, 2012.

Ehhalt, D. H., Dorn, H.-P. and Poppe, D.: The chemistry of the hydroxyl radical in the troposphere, Proc. R. Soc. Edinb. Sect. B Biol. Sci., 97, 17–34, https://doi.org/10.1017/S0269727000005273, 1990.

Gulz, P. G. and Boor, G.: Seasonal Variations in Epicuticular Wax Ultrastructures of Quercus robur Leaves, Z Naturforsch, 47c, 807–814, https://doi.org/10.1515/znc-1992-11-1205, 1992.

Kang, E., Root, M. J., Toohey, D. W. and Brune, W. H.: Introducing the concept of Potential Aerosol Mass (PAM), Atmos Chem Phys, 7(22), 5727–5744, https://doi.org/10.5194/acp-7-5727-2007, 2007.

Kreisberg, N. M., Hering, S. V., Williams, B. J., Worton, D. R. and Goldstein, A. H.: Quantification of Hourly Speciated Organic Compounds in Atmospheric Aerosols, Measured by an In-Situ Thermal Desorption Aerosol Gas Chromatograph (TAG), Aerosol Sci. Technol., 43(1), 38–52, https://doi.org/10.1080/02786820802459583, 2009.

Lambe, A. T., Ahern, A. T., Williams, L. R., Slowik, J. G., Wong, J. P. S., Abbatt, J. P. D., Brune, W. H., Ng, N. L., Wright, J. P., Croasdale, D. R., Worsnop, D. R., Davidovits, P. and Onasch, T. B.: Characterization of aerosol photooxidation flow reactors: heterogeneous oxidation, secondary organic aerosol formation and cloud condensation nuclei activity measurements, Atmos Meas Tech, 4(3), 445–461, https://doi.org/10.5194/amt-4-445-2011, 2011.

Levy, H.: Normal Atmosphere: Large Radical and Formaldehyde Concentrations Predicted, Science, 173(3992), 141–143, https://doi.org/10.1126/science.173.3992.141, 1971.

Li, R., Palm, B. B., Ortega, A. M., Hlywiak, J., Hu, W., Peng, Z., Day, D. A., Knote, C., Brune, W. H., de Gouw, J. A. and Jimenez, J. L.: Modeling the Radical Chemistry in an Oxidation Flow Reactor: Radical Formation and

Recycling, Sensitivities, and the OH Exposure Estimation Equation, J. Phys. Chem. A, 119(19), 4418–4432, https://doi.org/10.1021/jp509534k, 2015.

Manion, J. A., Huie, R. E., Levin, R. D., Burgess, D. R., Jr., Orkin, V. L., Tsang, W., McGivern, W. S., Hudgens, J. W., Knyazev, V. D., Atkinson, D. B., Chai, E., Tereza, A. M., Lin, C.-Y., Allison, T. C., Mallard, W. G., Westley, F., Herron, J. T., Hampson, R. F. and Frizzell, D. H.: NIST Chemical Kinetics Database, NIST Standard Reference Database 17, Version 7.0 (Web Version), Release 1.6.8, Data version 2015.12, [online] Available from: http://kinetics.nist.gov/

Mao, J., Ren, X., Brune, W. H., Olson, J. R., Crawford, J. H., Fried, A., Huey, L. G., Cohen, R. C., Heikes, B., Singh, H. B., Blake, D. R., Sachse, G. W., Diskin, G. S., Hall, S. R. and Shetter, R. E.: Airborne measurement of OH reactivity during INTEX-B, Atmos Chem Phys, 9(1), 163–173, https://doi.org/10.5194/acp-9-163-2009, 2009.

Mellott, P.: Development and Testing of Novel Atmospheric Chemistry Technologies, MS Thesis, Washington University in St. Louis, St. Louis, MO., 2012.

NIST Mass Spec Data Center, S.E. Stein, director: in NIST Chemistry WebBook, NIST Standard Reference Database Number 69, National Institute of Standards and Technology, Gaithersburg MD, 20899.

Ortega, A. M., Day, D. A., Cubison, M. J., Brune, W. H., Bon, D., de Gouw, J. A. and Jimenez, J. L.: Secondary organic aerosol formation and primary organic aerosol oxidation from biomass-burning smoke in a flow reactor during FLAME-3, Atmos Chem Phys, 13(22), 11551–11571, https://doi.org/10.5194/acp-13-11551-2013, 2013.

Palm, B. B., Campuzano-Jost, P., Ortega, A. M., Day, D. A., Kaser, L., Jud, W., Karl, T., Hansel, A., Hunter, J. F., Cross, E. S., Kroll, J. H., Peng, Z., Brune, W. H. and Jimenez, J. L.: In situ secondary organic aerosol formation from ambient pine forest air using an oxidation flow reactor, Atmos Chem Phys, 16(5), 2943–2970, https://doi.org/10.5194/acp-16-2943-2016, 2016.

Pankow, J. F.: An absorption model of gas/particle partitioning of organic compounds in the atmosphere, Atmos. Environ., 28(2), 185–188, https://doi.org/10.1016/1352-2310(94)90093-0, 1994.

Peng, Z., Day, D. A., Stark, H., Li, R., Lee-Taylor, J., Palm, B. B., Brune, W. H. and Jimenez, J. L.: HOx radical chemistry in oxidation flow reactors with low-pressure mercury lamps systematically examined by modeling, Atmos Meas Tech, 8(11), 4863–4890, https://doi.org/10.5194/amt-8-4863-2015, 2015.

Peng, Z., Day, D. A., Ortega, A. M., Palm, B. B., Hu, W., Stark, H., Li, R., Tsigaridis, K., Brune, W. H. and Jimenez, J. L.: Non-OH chemistry in oxidation flow reactors for the study of atmospheric chemistry systematically examined by modeling, Atmos Chem Phys, 16(7), 4283–4305, https://doi.org/10.5194/acp-16-4283-2016, 2016.

Reece, S. M., Sinha, A. and Grieshop, A. P.: Primary and Photochemically Aged Aerosol Emissions from Biomass Cookstoves: Chemical and Physical Characterization, Environ. Sci. Technol., 51(16), 9379–9390, https://doi.org/10.1021/acs.est.7b01881, 2017.

Shetter, R. E., Cantrell, C. A., Lantz, K. O., Flocke, S. J., Orlando, J. J., Tyndall, G. S., Gilpin, T. M., Fischer, C. A., Madronich, S., Calvert, J. G. and Junkermann, W.: Actinometric and radiometric measurement and modeling of the photolysis rate coefficient of ozone to O(1D) during Mauna Loa Observatory Photochemistry Experiment 2, J. Geophys. Res. Atmospheres, 101(D9), 14631–14642, https://doi.org/10.1029/96JD00211, 1996.

Stein, S. E. and Scott, D. R.: Optimization and testing of mass spectral library search algorithms for compound identification, J. Am. Soc. Mass Spectrom., 5(9), 859–866, https://doi.org/10.1016/1044-0305(94)87009-8, 1994.

Wong, Z., Chen, K. and Li, J.: Formation of Vanillin and Syringaldehyde in an Oxygen Delignification Process, BioResources, 5(3), 1509–1516, retrieved from https://bioresources.cnr.ncsu.edu, 2010.

Ziemann, P. J. and Atkinson, R.: Kinetics, products, and mechanisms of secondary organic aerosol formation, Chem. Soc. Rev., 41(19), 6582–6605, https://doi.org/10.1039/C2CS35122F, 2012.